Research Article

Paraskevi Z. Trialoni, Zografia-Christina M. Fyrigou, Christina N. Banti*, and Sotiris K. Hadjikakou*

Conjugation of tetracycline and penicillin with Sb(v) and Ag(i) against breast cancer cells

https://doi.org/10.1515/mgmc-2022-0016
received April 30, 2022; accepted July 01, 2022

Abstract: Tetracycline (**$TecH_2$**) reacts with triphenylantimony (**$TPSb^{iii}$**) in the presence of hydrogen peroxide to form the $[Ph_3Sb^{v}(Tec)]$ (**TecAn**). The sodium penicillin G (**PenH**) conjugates with Ag(i) towards $[Ag(Pen)(MeCN)]_2$ (**PenAcAg**). **TecAn** and **PenAcAg** were characterized by melting point, X-ray fluorescence spectroscopy, attenuated total reflectance-Fourier transform infra-red, thermogravimetric-differential thermal analysis in solid state, ultraviolet-Vis spectroscopy, and nuclear magnetic resonance (^{1}H and ^{13}C-NMR), spectroscopies in solution. The molecular weight was determined with cryoscopy. The *in vitro* cytotoxic activity of **TecAn** and **PenAcAg** was evaluated against the human breast adenocarcinoma cell lines: MCF-7 (positive to hormones receptor (HR+)), MDA-MB-231 (negative to hormones receptor (HR–)), and their *in vitro* toxicity and genotoxicity were tested against normal human fetal lung fibroblast cells (MRC-5). The MCF-7 cells' morphology and acridine orange/ethidium bromide staining suggest an apoptotic pathway for cell death. The binding affinity of **TecAn** and **PenAcAg** with DNA was, ex vivo, studied by UV-Vis and fluorescence spectroscopy and viscosity measurements of DNA solution. **PenAcAg** inhibits lipoxygenase (LOX) stronger than cisplatin, while no inhibitory activity has been detected for **TecAn**. The reduction of non-active Sb(v), of **TecAn**, to active Sb(iii) by glutathione (a tripeptide over expressed in tumor cells) was also investigated.

*** Corresponding author: Christina N. Banti,** Department of Chemistry, University of Ioannina, 45110 Ioannina, Greece, e-mail: cbanti@uoi.gr
*** Corresponding author: Sotiris K. Hadjikakou,** Department of Chemistry, University of Ioannina, 45110 Ioannina, Greece; Institute of Materials Science and Computing, University Research Center of Ioannina (URCI), 45110, Ioannina, Greece, e-mail: shadjika@uoi.gr
Paraskevi Z. Trialoni, Zografia-Christina M. Fyrigou: Department of Chemistry, University of Ioannina, 45110 Ioannina, Greece

Keywords: biological inorganic chemistry, organoantimony(v), silver(i), antibiotic, cytotoxicity, DNA–metal complexes interaction

1 Introduction

Although treatments have been evolved, breast cancer remains the most common malignancy in women (Llewellyna et al., 2019). Depending on the breast cancer cells' response to hormones, the disease is classified as hormone-dependent, when there is over expression of estrogen or progesterone receptors, or hormone-independent when the progression of the disease is independent to the hormone levels (The Cancer Genome Atlas Network, 2012).

Antibiotics promote cancer cell apoptosis, inhibit the growth, and prevent their metastasis (Gao et al., 2020). Among antibiotics, the group of anthracyclines have been studied for their antiproliferative activity (Gao et al., 2020). Doxorubicin, an antibiotic of anthracyclines family, has a broad anticancer spectrum (Gao et al., 2020). It is widely used to treat various types of cancer, including breast cancer (Christowitz et al., 2019). Its mechanism involves breakage of DNA strands, since DNA is one of the major molecular targets of antibiotics (Gao et al., 2020; Rocha et al., 2018). Besides, tetracycline exhibits structural similarity to doxorubicin (Fuoco, 2012; Mealey et al., 2002). *N*-Methylthio β-lactams, on the other hand, is a class of drugs that have been found to induce apoptosis in several cancer cell lines, including breast, prostate, head, and neck cancers, and leukemia (Bhattacharya and Mukherjee, 2015). Penicillin is the most common beta-lactam antibiotic (Macy, 2014). Therefore, it is of interest to investigate whether an antiproliferative activity of conjugates of tetracycline or penicillin with main group metals and/or metals is exhibited as well.

Antimonials are used for the treatment of fever, pneumonia, inflammatory diseases, and leishmaniasis (Ozturk et al., 2014; Polychronis et al., 2019). Although, Sb(iii) compounds are more active than those of Sb(v), the

latter are used as pro-drugs due to their lower toxicity. Once these compounds enter into cytoplasm, Sb(V) is reduced to Sb(III) due to the specific microenvironmental conditions of cancer cells, like the low O_2 level or the presence of the tripeptide glutathione (GSH). GSH is over expressed in the cancerous cells participating in the cell resistance mechanism (Polychronis et al., 2019). Silver(I) compounds, on the other hand, interact with nuclear DNA and lipoxygenase (LOX), causing cells' apoptosis through the mitochondrial signaling pathway (Banti et al., 2016). Recently, the conjugate of penicillin G (PenH) with silver(I) ions with formula $[Ag(pen)(MeOH)]_2$ (**PenAg**) was synthesized, characterized, and studied for its antibacterial activity against Gram negative and positive bacterial strains (Ketikidis et al., 2020).

In the course of our studies in the field of drug design and development of new chemotherapeutics for breast cancer treatment (Banti et al., 2015, 2016, 2021; Chrysouli et al., 2018; Ketikidis et al., 2020; Latsis et al., 2018; Polychronis et al., 2019; Stathopoulou et al., 2021; Tsiatouras et al., 2016), from the conjugation of antibiotics or non-steroidal anti-inflammatory drugs (NSAIDs) with metal ions, here we report the conjugation of $TecH_2$ and PenH (Scheme 1), with antimony(V) and silver(I), respectively, with formulae $[Ph_3Sb(Tec)]$ (**TecAn**) and $[Ag(Pen)(MeCN)]_2$ (**PenAcAg**). The new compounds were characterized by melting point, X-ray fluorescence spectroscopy (XRF), attenuated total reflectance-Fourier transform infra-red (ATR-FTIR), thermogravimetric-differential thermal analysis (TG-DTA), ultraviolet-visible (UV-Vis) spectroscopy, nuclear magnetic resonance (^{1}H and ^{13}C-NMR). **PenAcAg** is also obtained by the already known $[Ag(Pen)(MeOH)]_2$ (**PenAg**) by its treatment with acetonitrile (Ketikidis et al., 2020). The *in vitro* cytotoxicity of **TecAn** and **PenAcAg** was evaluated towards MCF-7 and MDA-MB-231 cell lines. The *in vitro* toxicity and genotoxicity of both compounds were also tested against MRC-5 cell line. The apoptotic type of MCF-7 cell death was confirmed by cell morphology and acridine orange/ethidium bromide (AO/EB) staining. The *ex vivo* mechanism of **TecAn** and **PenAcAg** was clarified by CT-DNA interaction studies and LOX studies. In the case of **TecAn**, its reaction with GSH was also evaluated.

2 Results and discussion

2.1 General aspects

TecAn was synthesized by reacting $TecH_2$ with Ph_3Sb in the presence of hydrogen peroxide (Scheme 2). The pale-yellow precipitation was filtered off and dried in room temperature. **PenAcAg** was obtained by reacting equimolar amount of silver nitrate ($AgNO_3$) with the sodium salt of penicillin G (PenNa) (1:1) in double distilled water (ddw) (Scheme 2) (Ketikidis et al., 2020). The powder products are purified by dissolving them in acetonitrile following by centrifugation at 2,000 rpm. The clear supernatant solutions were concentrated in the rotary evaporator to dryness and the yellow solids **TecAn** and **PenAcAg** were collected with diethylether (Et_2O). Several attempts have been made to grow crystals using various solvents and crystallization methods without success. **TecAn and PenAcAg** are air stable when are stored in darkness at room temperature. **TecAn** is highly soluble in CH_2Cl_2, $CHCl_3$, DMF, Dimethylsulfoxide (DMSO), and acetone and soluble in

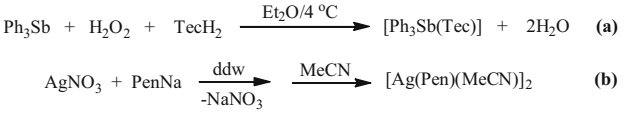

Scheme 2: Reaction route for the synthesis of **TecAn** (a) and **PenAcAg** (b).

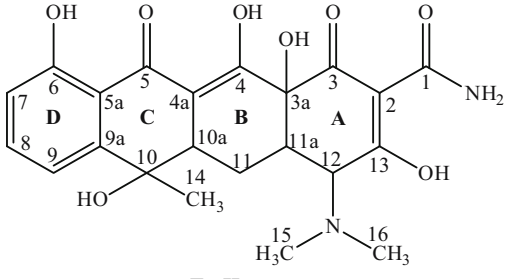

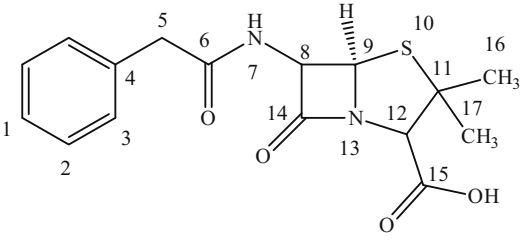

Scheme 1: Molecular diagram of $TecH_2$ and PenH.

MeOH and MeCN, while **PenAcAg** is highly soluble in CH_2Cl_2, $CHCl_3$, MeCN, DMF, and DMSO and soluble in MeOH.

2.2 XRF spectroscopy

The XRF spectrum of **TecAn** powder confirms the presence of Sb in the complex (Figure 1). The content of Sb in **TecAn** was determined at 14.86 (±0.09)% w/w (calc. for [Ph_3Sb(Tec)] 15.31% w/w). The content of Ag in the case of **PenAcAg** was found 19.81 (±0.27)% w/w (calc. for $[Ag(Pen)(MeCN)]_2$ 22.4% w/w).

2.3 Cryoscopic molecular weight (MW) measurements

The MWs of the compounds were measured with cryoscopy in DMSO/ddw (1:49 v/v) solution using freezing point osmometer. A solution of 1 μL **TecAn** or **PenAcAg** (1 mg/100 μL DMSO) was diluted to 50 μL ddw. The MW was found to be 799 g·mol^{-1} for **TecAn** (calc. 795.5 g·mol^{-1} for [Ph_3Sb(Tec)]) and 912 g·mol^{-1} for **PenAcAg** (calc. 946 g·mol^{-1} for $[Ag(Pen)MeCN]_2$).

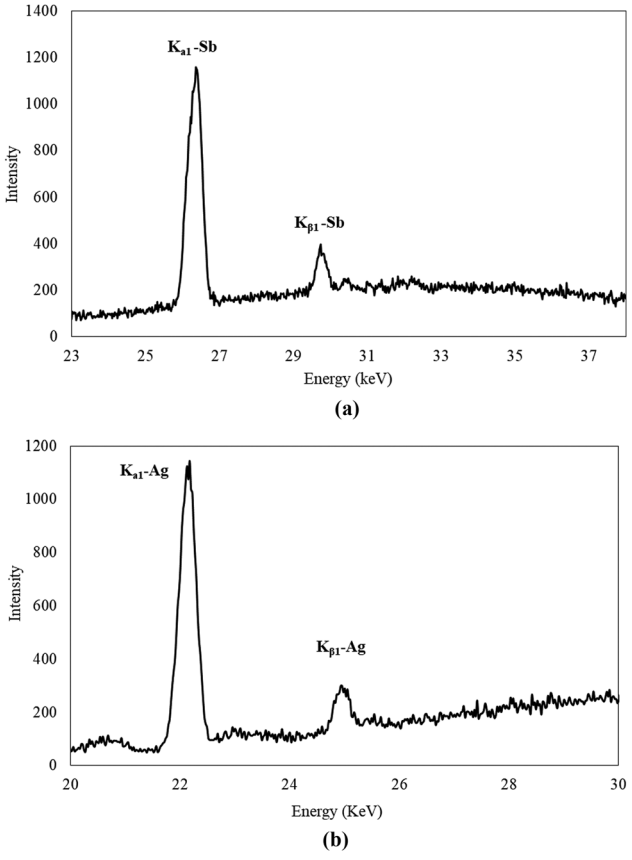

Figure 1: XRF spectra of **TecAn** (a) and **PenAcAg** (b).

2.4 ATR-FTIR

The ν(H–$C_{aromatic}$) and ν(H–$C_{aliphatic}$) bands in the IR spectrum of **$TecH_2$** at 3,050 and 2,958 cm^{-1}, respectively, (Leypold et al., 2003) are observed in the spectrum of **TecAn** (Figures S1–S3 in Supplementary material). The vibrational band at 1,640 cm^{-1} in the FTIR spectrum of tetracycline is assigned to the ν(amid-CO) and ν(O=C(3)) vibration bands (Scheme 1) (Leypold et al., 2003). This band is shifted by 12 cm^{-1} (at 1,652 cm^{-1}) in the spectrum of **TecAn** implying coordination of **$TecH_2$** to Sb(v) through either the amide O(C1) or the carbonyl O(C3) donor atom. The vibrational bands at 1,328 and 1,302 cm^{-1} in the IR spectrum of **$TecH_2$** are attributed to the O–C(13) and H–OC(13) bond vibrations (Scheme 1) (Leypold et al., 2003). These bands are observed at 1,335 and 1,302 cm^{-1} in the spectrum of **TecAn** indicating the non-involvement of the O[C(13)] atom in the coordination to Sb. The vibrational band at 410 cm^{-1} in the IR spectrum of **TecAn** is assigned to the Sb–O bond vibration (Bordner et al., 1986). Therefore, a coordination of $TecH_2$ to Sb(v) through amide C(1) and carbonyl C(3) oxygen atoms is concluded by ATR-FTIR spectroscopy.

The assignment of the FTIR spectrum of **PenAcAg** was based on the already reported one (Anacona and Figueroa, 1999; Ketikidis et al., 2020). Briefly, the ν_{as} (–COO–) and ν_s(–COO–) of the carboxylic group in the IR spectrum of PenNa at 1,619 and at 1,416 cm^{-1} (Figure S4) are shifted in the case of **PenAcAg** at 1,576 and 1,394 cm^{-1}, respectively (Figure S5) (Anacona and Figueroa, 1999; Ketikidis et al., 2020). The $\Delta\nu$ [$\nu_{as}(COO^-)$–ν_s (COO^-)] difference value of the ionic salt of penicillin PenNa is 203 cm^{-1}, while the corresponding value $\Delta\nu$ for **PenAcAg** is 182 cm^{-1} supporting the coordination of the ligand to the metal center through the carboxylic acid group. Taking into consideration that the $\Delta\nu$ of **PenAcAg** is close to the corresponding one of PenNa, a bridging coordination mode of the carboxylic group of penicillin G to Ag(I) is concluded. This is in accordance with the structure already proposed for $[Ag(Pen)MeOH]_2$ (Anacona and Figueroa, 1999; Ketikidis et al., 2020). The vibration band of the keto-group (C=O) of β-lactam at 1,774 cm^{-1} in PenNa remains unchanged in **PenAcAg** (at 1,767 cm^{-1}) suggesting no involvement of this group in the coordination of PenNa

into Ag(I). Thus, PenNa coordinating to Ag(I) through carboxylic group in a bridging mode is concluded by ATR-FTIR spectroscopy.

2.5 TG-DT analysis

TG/DTA analysis was performed under air flow with a rate of 10°C·min^{-1} up to 500°C. Two main decompose endothermic steps are observed in the case of **TecAn**: the first one occurs at 170–200°C with 10.3% mass loss which corresponds to the evolution of one phenyl group (Ph-H) from TPSb (calc. 9.8%) and the second one at 200–285°C with mass loss 19.3% which corresponds to the evolution of two phenyl groups (Ph-H) of TPSb (calc. 19.6%) (Figure S6). The TG/DTA thermograph shows that **PenAcAg** decomposes in two steps: the first is observed at 70–140°C with 6.7% mass loss which corresponds to the evolution of one acetonitrile (calc. 8.5%) and the second occurs at 150–140°C with 57.3% which corresponds to the evolution of one PenH (calc. 69%) (Figure S7).

2.6 UV-Vis spectroscopy

The UV-Vis absorption spectra of **TecAn**, **TPSb**, and **$TecH_2$** were recorded in DMSO solution (Figure S8). Two absorption bands at 368 nm (ε = 17,104 cm^{-1}·M^{-1}) and 266 nm (ε = 25,080 cm^{-1}·M^{-1}) are observed in the spectrum of **$TecH_2$**, which are assigned to $\pi^* \leftarrow \pi$ transitions. The spectrum of **TPSb** is dominated by one absorption band at 266 nm (ε = 10,740 cm^{-1}·M^{-1}) which is attributed to $\pi^* \leftarrow \pi$ electrons excitation. The corresponding spectrum of **TecAn** shows three absorption bands at 378 nm (ε = 16,270 cm^{-1}·M^{-1}), at 304 nm (ε = 13,964 cm^{-1}·M^{-1}) and at 266 nm (ε = 13,116 cm^{-1}·M^{-1}). The new absorption band at 304 nm (ε = 13,968 cm^{-1}·M^{-1}) in the spectrum of **TecAn** is assigned to metal to ligand charge transfer transition. The bands at 378 and 266 nm are assigned to intraligand $\pi^* \leftarrow \pi$ transitions. The corresponding UV-Vis spectra of **PenAcAg** and **PenH** in DMSO solution show one transition band at λ_{max} 269 nm (ε = 5,795 cm^{-1}·M^{-1}) which is assigned to intraligand $\pi^* \leftarrow \pi$ transitions and 262 nm (ε = 1,310 cm^{-1}·M^{-1}), respectively (Figure S9)

2.7 Stability studies

The stability of **TecAn** and **PenAcAg** in DMSO-d_6 solution was tested by ^{1}H-NMR spectroscopy (Figures S10 and S11) for 48 h. No changes were observed between the initial ^{1}H-NMR spectra and the corresponding ones recorded after 48 h, confirming the retention of the structures of both **TecAn** and **PenAcAg** in solution.

2.8 ^{1}H-NMR studies

2.8.1 TecAn

The ^{1}H-NMR spectra of $TecH_2$, TPSb, and **TecAn** in DMSO-d_6 are shown in Figure 2 and Figure S12. The broad resonance signals at 9.15 and 8.78 ppm in the spectrum of $TecH_2$ are attributed to the amide H[NH_2–C(1)=O] (Scheme 1) protons (Williamson and Everett, 1975). These signals are observed at 9.21 and 9.25 ppm, respectively, in the spectrum of **TecAn**. The resonance signals at 7.54 ppm in the spectrum of $TecH_2$ is assigned to the H[$C(8)_{aromatic}$] of D ring (Scheme 1), at 7.12 ppm is attributed to the H[$C(9)_{aromatic}$] (Scheme 1), and the signal at 6.91 ppm corresponds to the H[$C(7)_{aromatic}$] (Scheme 1) (Williamson and Everett, 1975). Upon coordination of $TecH_2$ to Sb(V) ion in **TecAn**, these signals are shifted upfield at 7.37, 7.00, and 6.77 ppm respectively, suggesting deprotonation of the hydroxyl H[O–C(6)] group. The aromatic protons of the phenyl groups of TPSb appear at 7.39–7.31 ppm. These signals are observed at 7.74–7.62 (o-H[Ph-Sb]) and 7.44–7.42 ppm (p-H[Ph-Sb]) in the spectrum of **TecAn**. The broad signal at 5.06 ppm in the spectrum of $TecH_2$ corresponds to the hydroxyl H[O–C(10)] proton (Williamson and Everett, 1975), which is observed at 4.88 ppm in the spectrum of **TecAn**. The resonance signal at 2.87 ppm in the spectrum of $TecH_2$ is assigned to H[C(10a)] proton, while the signal at 2.0 ppm is assigned to the H[C(11)] proton (Scheme 2). These signals are observed at 2.87 and at 2.04 ppm, respectively, in the spectrum of **TecAn**. The signal at 2.41 ppm corresponds to the H[H_3C(15)] and H[H_3C(16)] of $TecH_2$, while it appears at 2.61 ppm in **TecAn**. The signal at 1.50 ppm is attributed to the methyl protons of H[H_3C(14)] and it remains unchanged. Assignment of the ^{1}H-NMR spectrum of **TecAn** results in the $\Delta\delta$ values with respect to the corresponding ones in $TecH_2$ in DMSO-d_6 (Figure 3). The protons that strongly shifted are H[NH–C(1)=O], H[H_3C(15)] and H[H_3C(16)] due to the coordination of $TecH_2$ to Sb through amide and carbonyl oxygen atoms (Scheme 1). The integration of the o-H[Ph-] of phenyl substituent of TPSb in **TecAn** (6 protons) with those of methylene H[C(14)] (3 protons) confirms the 1:1 molar ratio of Sb:$TecH_2$ in **TecAn** (Figure 2).

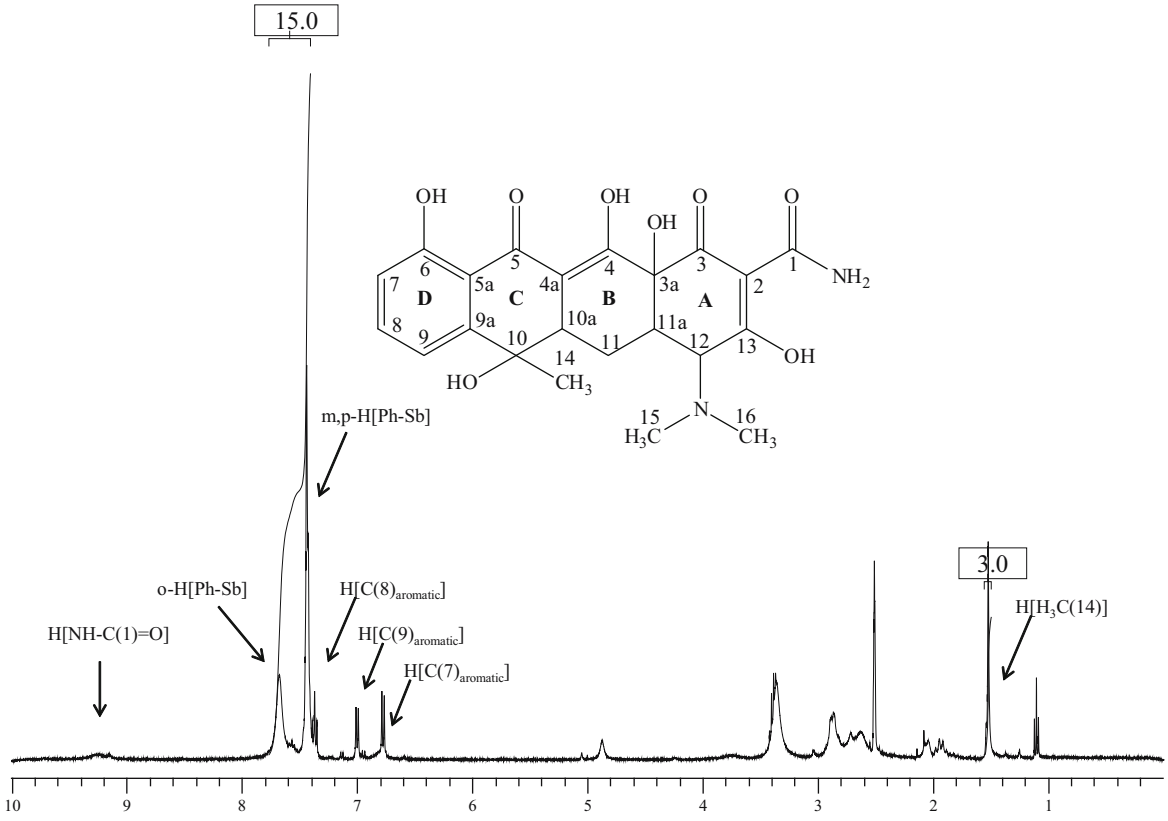

Figure 2: ^{1}H-NMR spectra of **TecAn** in DMSO-d_6.

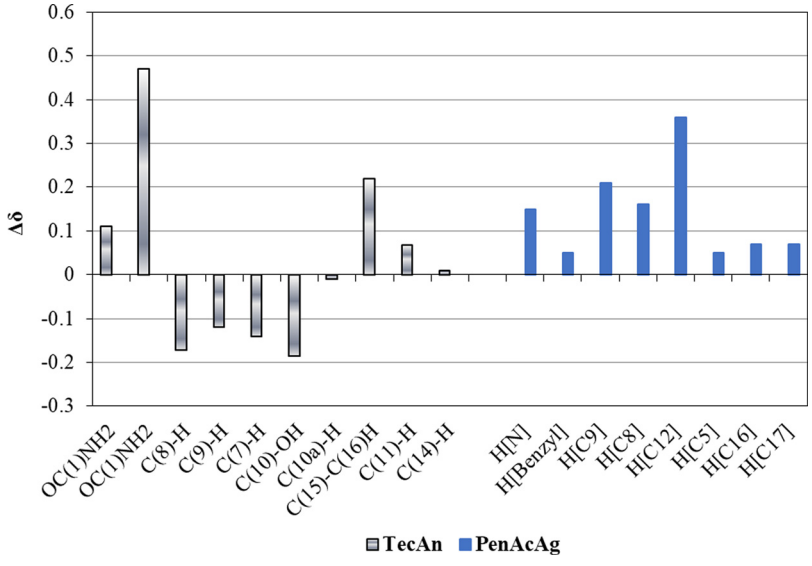

Figure 3: The Δδ values in ^{1}H-NMR of **TecAn** and **PenAcAg** with respect to the corresponding ones in TecH2 and PenNa in DMSO-d_6.

2.8.2 PenAcAg

The ^{1}H-NMR spectra of PenNa and **PenAcAg** in DMSO-d_6 are shown in Figure 4 and Figure S13. The resonance signal at 8.66 ppm in the spectrum of **PenNa** is attributed to the amide proton H[NH–C(6)═O] (Scheme 1) (Branch et al., 1987). This signal is shifted at 8.81 ppm in the spectrum of **PenAcAg.** The resonance signals at 7.29–7.17 ppm in the spectrum of PenNa are assigned to the aromatic protons of the benzyl group (Scheme 1) (Ben Salem et al.,

2016). These signals are observed at 7.32–7.22 ppm in the case of **PenAcAg**. The signals at 5.26 ppm and 5.28 ppm in the spectrum of PenNa are assigned to H[C(9)] proton and H[C(8)] proton, respectively (Ben Salem et al., 2016). These signals are downfield shifted at 5.48 and at 5.40 ppm, respectively, in the spectrum of **PenAcAg**. The resonance signal at 3.78 ppm corresponds to the H[C(12)] proton of PenNa, while for **PenAcAg** it appears at 4.14 ppm. This strong shift ($\Delta\delta$ = 0.36) confirms the coordination of the carboxylic group with the Ag(I). The signal at 3.5 ppm is attributed to H[C5] proton (Figure 3) (Ben Salem et al., 2016) and remains unshifted in **PenAcAg**. The resonance signal to 2.09 ppm is assigned to H[CH_3CN] of the coordinated acetonitrile to the Ag(I). The corresponding signal of free H[MeCN] is observed at 2.07 ppm (Gottlieb et al., 1997). The resonance signals at 1.53 and 1.41 ppm are attributed to H[C(16)] and H[C(17)] protons (Ben Salem et al., 2016), respectively, while in the spectrum of **PenAcAg** they appear at 1.60 and 1.48 ppm, respectively. The $\Delta\delta$ values between PenNa and **PenAcAg** in DMSO-d_6 are shown in Figure 3. The protons that strongly shifted are H[C(12)] H[C(9)] and H[C(8)] due to the coordination of PenH to Ag through carboxylic oxygen atoms Sb (Scheme 1). The integration of the H[C(16)] (3 protons) with those of H[MeCN] (3 protons) confirms the 1:1 molar ratio of Ag:PenH in **PenAcAg** (Figure 4).

2.9 Molecular structure elucidation

Based on the analytical and spectroscopic data from XRF, cryoscopy, FTIR, and ^{1}H-NMR the following possible formulae (Scheme 3) can be concluded for **TecAn** and **PenAcAg**.

2.10 Biological studies

2.10.1 *In vitro* antiproliferative activity

The *in vitro* antiproliferative activity of **TecAn** and **PenAcAg** was tested against two human adenocarcinoma breast cell

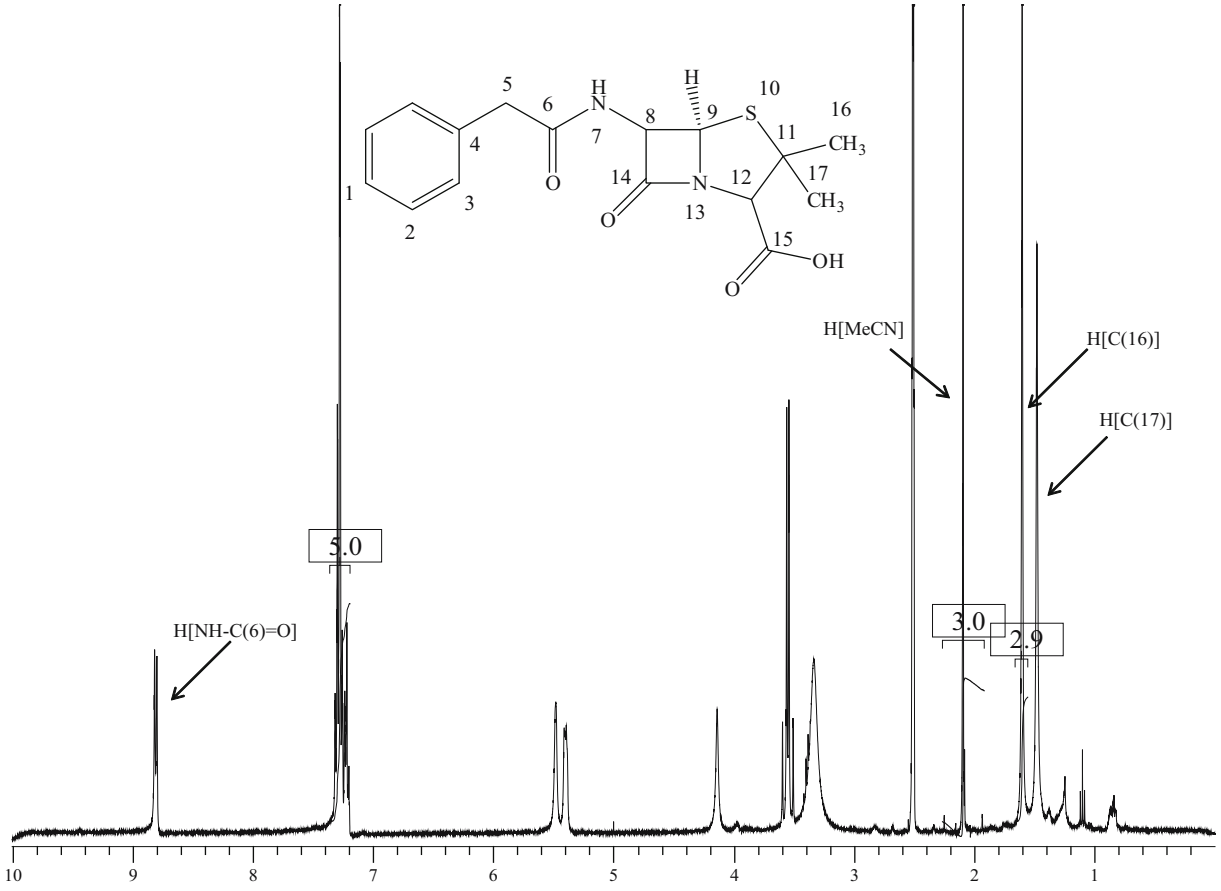

Figure 4: ^{1}H-NMR spectra of **PenAcAg** in DMSO-d_6.

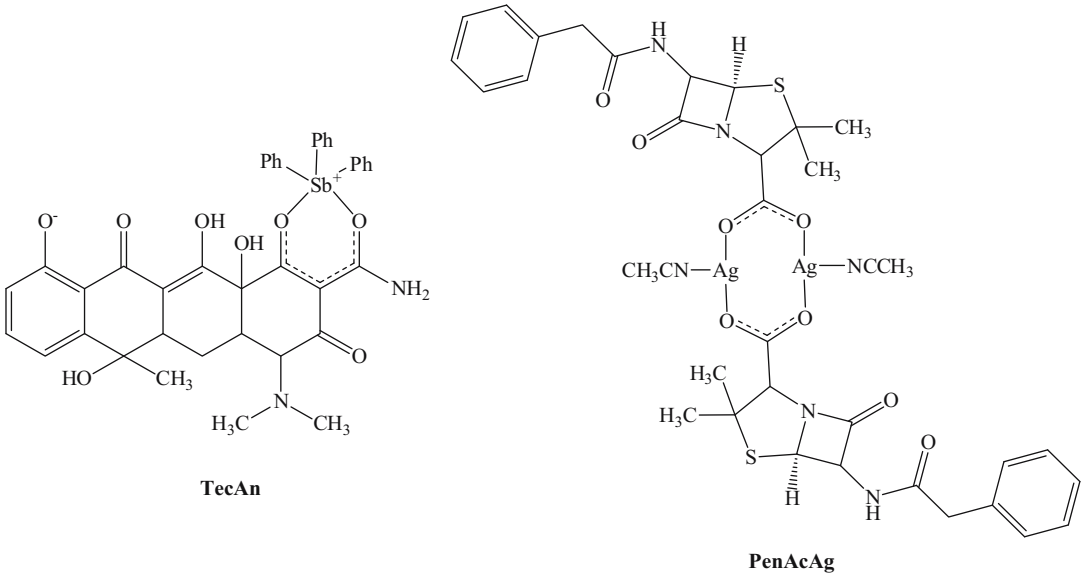

Scheme 3: A possible formulae of **TecAn** and **PenAcAg** with charge distribution.

lines, MCF-7 (hormone depended (HD)) and MDA-MB-231 (hormone independent (HI)) by sulforhodamine B (SRB) assay after their incubation for 48 h. The IC_{50} values of **TecAn** and **PenAcAg** against MCF-7(HD) are 26.0 ± 1.4 and 8.1 ± 0.2 μM, respectively, while the corresponding values against MDA-MB-231(HI) are 27.8 ± 0.9 and 8.9 ± 0.2 μM, respectively (Table 1). The antibiotics $TecH_2$ and PenNa were inactive against both cell lines in the concentrations tested (up to 40 μM) (Table 1). Therefore, the conjugation of tetracycline with TPSb and penicillin with Ag(I) enhances their antiproliferative activity. The IC_{50} values of cisplatin are 6.8 ± 0.3 μM (MCF-7(HD)) and 26.7 ± 1.1 μM (MDA-MB-231(HI)). Hence, **PenAcAg** reveals 3-folds stronger activity than cisplatin against MDA-MB-231(HI) malignant cells. Both agents exhibit similar activity against MCF-7 (HD) and MDA-MB-231(HI) cells suggesting that hormone receptors might not involve in their mechanism of action.

2.10.2 *In vitro* toxicity study

The toxicities of **TecAn** and **PenAcAg** were examined against normal human fetal lung fibroblast cells (MRC-5). Their IC_{50} values of **TecAn** and **PenAcAg** against MRC-5 cells are 24.5 ± 1.0 and 7.9 ± 0.2 μM, respectively, while the corresponding value of cisplatin is 1.1 ± 0.2 μM. The Therapeutic Potency Index (TPI), which is defined as the IC_{50} of an agent against non-cancerous cells toward its IC_{50} against cancerous cells, for **TecAn** and **PenAcAg** are 0.94 and 0.98 against MCF-7 (HD) and 0.88 and 0.89 against MDA-MB-231(HI), respectively (Table 1). Given that the corresponding TPI values of cisplatin against MCF-7 (HD) and MDA-MB-231(HI) are 0.20 and 0.04, **TecAn** and **PenAcAg** are significantly more effective against cancerous than normal cells from cisplatin. Moreover, US Food and Drug Administration (FDA) defines an agent with no selectivity when it exhibits minimum toxic concentration (MTC)/minimum effective concentration (MEC) value less than 2 (Abughazaleh and Tracy, 2014). Thus, both **TecAn** and **PenAcAg** should be considered as toxic agents as well as cisplatin which however is an anticancer drug with clinical use.

2.10.3 *In vitro* genotoxicity study

The *in vitro* genetic damage caused by **TecAn** and **PenAcAg** towards MRC-5 cells was evaluated by the micronucleus (MN) assay. MNs are formed during the metaphase anaphase transition of the mitosis of a normal cell under the influence of a xenobiotic agent (such as chemicals) (Banti et al., 2021). The MRC-5 cells were incubated by **TecAn** and **PenAcAg** at their IC_{50} value. The MN frequency of the untreated cells is 1.0 ± 0.3%. When the MRC-5 cells were treated with **TecAn**, the MN frequency is 1.6 ± 0.1%, showing similar genotoxicity with that of control, while the MN is 2.0 ± 0.4%, when **PenAcAg** is used. The genotoxicity caused by **TecAn** and **PenAcAg** is similar than that of cisplatin, (MN frequency 1.6%) (Banti et al., 2016) (Figure 5).

2.10.4 *In vivo* toxicity studies

In order to examine the *in vivo* toxicity of **TecAn**, the brine shrimp *Artemia salina* assay was used (Banti and

Table 1: Antiproliferative activity of compounds against MCF-7 (HD), MDA-MB 231 (HI), and MRC-5 cells

	IC_{50} (μM)			TPI		K_b ($\times 10^4$) M^{-1}	K_{app} ($\times 10^4$) M^{-1}	LOX inhibition IC_{50} (μM)	Ref.
	MCF-7	**MDA-MB 231**	**MRC-5**	**MCF-7**	**MDA-MB 231**				
TecAn	26.0 ± 1.4	27.8 ± 0.9	24.5 ± 1.0	0.94	0.88	11.1 ± 0.5	1.1 ± 0.2	>60	*
$TecH_2$	>40	>40	>40			7.2 ± 0.8	0.8 ± 0.4	>40	*
Ph_3Sb	>30	>30	>30			—	5.3 ± 0.5	ND	(Banti et al., 2016)
PenAcAg	8.1 ± 0.2	8.9 ± 0.2	7.9 ± 0.2	0.98	0.89	15.6 ± 5.1	6.7 ± 1.1	19.8	*
PenNa	>30		>30			—	0.9 ± 0.1	>40	*
$[Ph_3Sb(Carv)_2]$	7.1 ± 0.2	7.2 ± 0.3	8.1 ± 0.3	1.1	1.1	—	3.10 ± 0.43	ND	(Kapetana and Banti, 2022)
$\{[Ph_3Sb(SalH)]_2O\}$	11.9 ± 0.6	8.0 ± 0.4	7.8 ± 0.2	0.7	1.0	30 ± 5.0	ND	NA	(Polychronis et al., 2019)
Cisplatin	5.5 ± 0.4	26.7 ± 1.1	1.1 ± 0.2	0.20	0.04			65.9	(Banti et al., 2016)

*This work; Carv = carvacrol; SalH2 = salicylic acid; NA = no activity; ND = not determined.

Hadjikakou, 2021). This assay is selected because it can predict a variety of biological activities of an agent, such as cytotoxic, phototoxic, pesticidal, and pharmacological activities of bioactive compounds (Banti and Hadjikakou, 2021; Stathopoulou et al., 2021). Therefore, several characteristics of brine shrimp such as its widespread distribution, short life cycle, non-selective grazing, and sensitivity to toxic substances (Banti and Hadjikakou, 2021), make it the ideal candidate to conduct this test.

The survival rate (%) of *Artemia salina* larvae in increasing concentrations of solutions with or without **TecAn** and $TecH_2$ after 24 h is evaluated and the lethality was noted in terms of deaths of larvae. The concentrations used were 25, 50, and 100 μM. For the compounds the survival rates are up to 100% at all concentrations although it rises even up to 4-fold higher than the IC_{50} values for **TecAn**. No mortality rate of brine shrimp larvae was found upon their incubation with **PenAg** in concentrations up to 220 μM (Ketikidis et al., 2020). This survival rate indicates no toxicity of **TecAn** and **PenAg** at their IC_{50} values and at higher concentrations (Ketikidis et al., 2020).

2.10.5 *In vitro* mechanism of action

The mechanism of action of **TecAn** and **PenAcAg** against MCF-7 (HD) cells was examined *in vitro* by the means of cell morphology studies and AO/EB Staining. Moreover, the molecular mechanism was further studied *ex vivo* by their binding affinity towards CT-DNA using UV-Vis, fluorescence spectroscopy, and viscosity studies. The inhibitory activity of **TecAn** and **PenAcAg** towards LOX, an enzyme which catalyzes the oxidation of linoleic acid to hydroperoxy linoleic acid during the inflammation process, is also studied *ex vivo*. The low active antimonials(v) pro-drugs, such as **TecAn**, on the other hand, can readily be converted to the active drugs Sb(III) by GSH. GSH is a tripeptide that is over-expressed in tumor cells, and it is involved in the development of cancer cells' resistance to chemotherapeutics drugs. The redox reaction between the GSH and **TecAn** is studied, here, using vibrational spectroscopy.

2.10.5.1 Cell morphology studies

MCF-7 cells are treated with **TecAn** and **PenAcAg** at their IC_{50} values for 48 h and they are observed in inverted microscope, in order to assess the type of their death by their morphology. Figure 6 shows the morphological

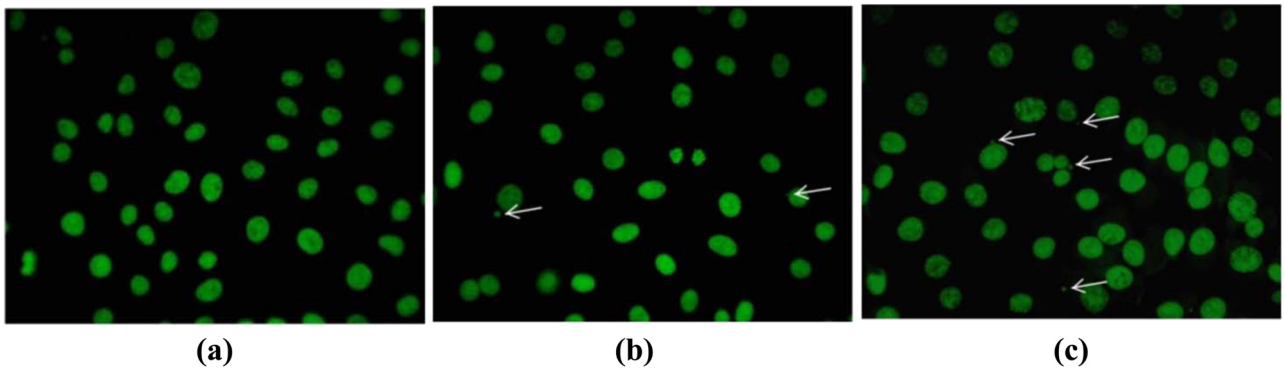

Figure 5: Snapshots of MN formed in untreated MRC-5 cells (a) and upon their treatment with **TecAn** (b) and **PenAcAg** (c) for 48 h.

changes. The proliferation of the untreated MCF-7 (HD) cells is normal since they are elongated, adherent, and showed cellular crowding. However, the morphology of those treated with **TecAn** and **PenAcAg** was altered. The cells lost their characteristic morphology, were shrunk and rounded, were detached from the plate, the cell contact was lost, and they formed islets of more rounded cells in contrast to the untreated cells (Banti et al., 2016, 2021; Kapetana and Banti, 2022; Stathopoulou et al., 2021). Therefore, an apoptotic type of cell death is assumed after the treatment of MCF-7 cells with **TecAn** and **PenAcAg**.

2.10.5.2 AO/EB staining assay

The apoptotic or necrotic cell death was evaluated with the AO/EB staining assay. The nuclear changes and apoptotic body formation are characteristic of the cascade of apoptosis (Naqvi et al., 2017). AO is a cell permeable fluorescent dye and stains nuclear DNA in both live and dead cells, while EB is a fluorescent dye that only stains nuclear DNA in cells which have lost their membrane integrity (Afsar et al., 2016). In this way, four different cell types, according to the fluorescence emission and the morphological features of the stained nuclei, are observed. (i) viable cells are uniformly stained green, (ii) early apoptotic cells are stained greenish yellow or displayed green yellow fragments, (iii) late apoptotic cells are stained orange or displayed orange fragments, and (iv) necrotic cells show orange to red fluorescing nuclei with no indication of chromatin fragmentation, uniformly red fluorescing, and the cells were swollen to large size (Afsar et al., 2016).

The untreated MCF-7 cells identified by bright uniform green nuclei with organized structures are shown in Figure 7. The percentage of apoptosis and necrosis in the control group was calculated to be 26.8 ± 1.5% and 0%, respectively. In the case of the treated cells with **TecAn** and **PenAcAg**, a shrinkage, chromatin condensation, and blebbing of the plasma membrane is observed, indicating that the majority of the cells undergoes apoptotic cell death (Figure 7) (Jaksic, 2012). The percentage of apoptotic and necrotic cells upon treatment with **TecAn** and **PenAcAg** are

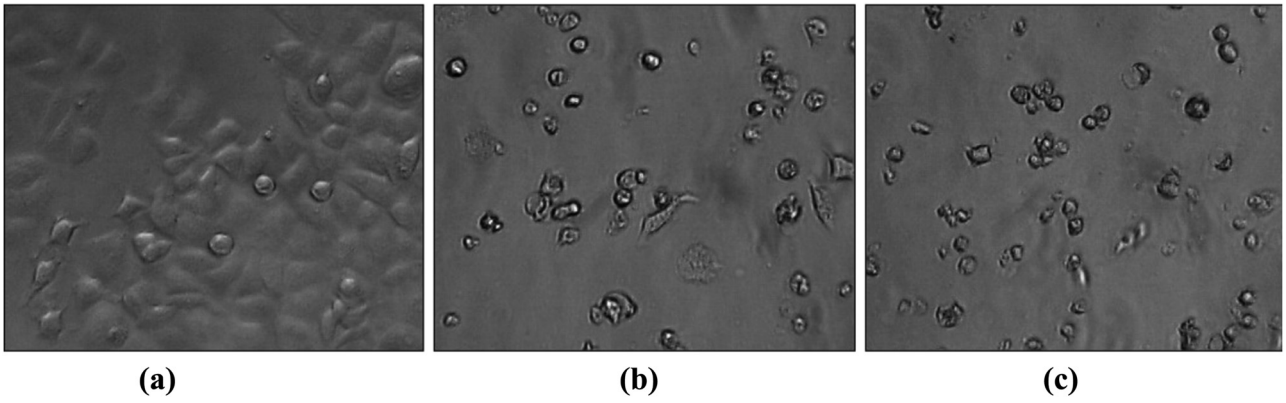

Figure 6: Morphological alterations observed in the untreated MCF-7 cells (a), treated with **TecAn** (b), and **PenAcAg** (c).

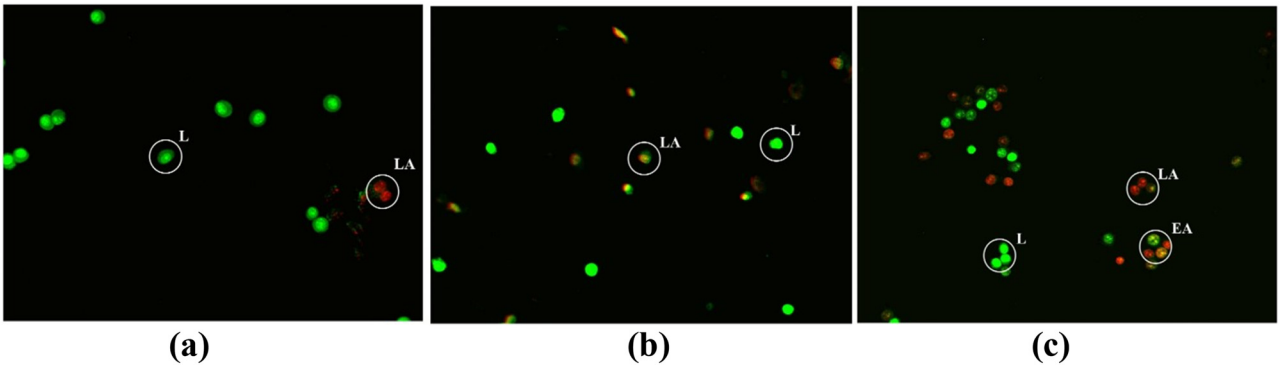

Figure 7: Fluorescence images of the untreated MCF-7 cells (a), treated with **TecAn** (b), and **PenAcAg** (c) for 48 h at 37°C at IC_{50} values and stained with AO/EB. "L" indicates live cells; "EA" indicates early apoptotic cells; "LA" indicates late apoptotic cells.

56.2 ± 0.2% and 0% (**TecAn**) and 49.3 ± 0.6% and 0% (**PenAcAg**), respectively. When MCF-7 cells are incubated with cisplatin, the percentage of apoptotic cells rises up to 96.5%. Therefore, **TecAn** and **PenAcAg** induce apoptosis but not in the magnitude that cisplatin does.

2.11 *Ex vivo* studies

2.11.1 DNA binding studies

2.11.1.1 UV-Vis absorption spectroscopic studies

In order to examine the binding efficiency of **TecAn** and **PenAcAg** towards CT-DNA, UV-Vis absorption spectroscopy was employed (Banti et al., 2016, 2021). There are three types of non-covalent interactions which are studied by UV-Vis spectra: (i) electrostatic interaction with the negatively charged nucleic sugar–phosphates, (ii) groove binding interaction with the grooves of DNA double helix, and (iii) intercalative interaction between the stacked base pairs of native DNA (Banti et al., 2016, 2021). Changes in the configuration of the DNA double helix results in hypochromic and hyperchromic effects; hypochromism shows intercalated or electrostatic binding mode, while hyperchromism is the breakage of hydrogen bonds or groove binding of the compound with the DNA. Moreover, shifting in λ_{max} to higher wavelengths (red shift) suggests stabilization of the helical structure of DNA and shifting of λ_{max} to shorter wavelengths (blue shift) indicates destabilization of the helical structure of DNA (Banti et al., 2016, 2021; Psomas, 2008).

A significant increase in the absorption intensity of DNA solution at λ_{max} = 258 nm, upon treatment with the **TecAn** and **PenAg** at various *r* values (*r* = [complex]/[DNA]) in a constant [DNA] = 10^{-4} M is observed (hyperchromism: 13.9% (**TecAn**) and 9.9% (**PenAg**)) (Figure 8). This indicates either breakage of hydrogen bonds or groove binding between CT-DNA and **TecAn** or **PenAg**.

The binding constant (K_b) of **TecAn** and **PenAg** towards CT-DNA was evaluated by monitoring the changes in absorbance of the UV spectra of the agent, ([agent] = 10 μM),

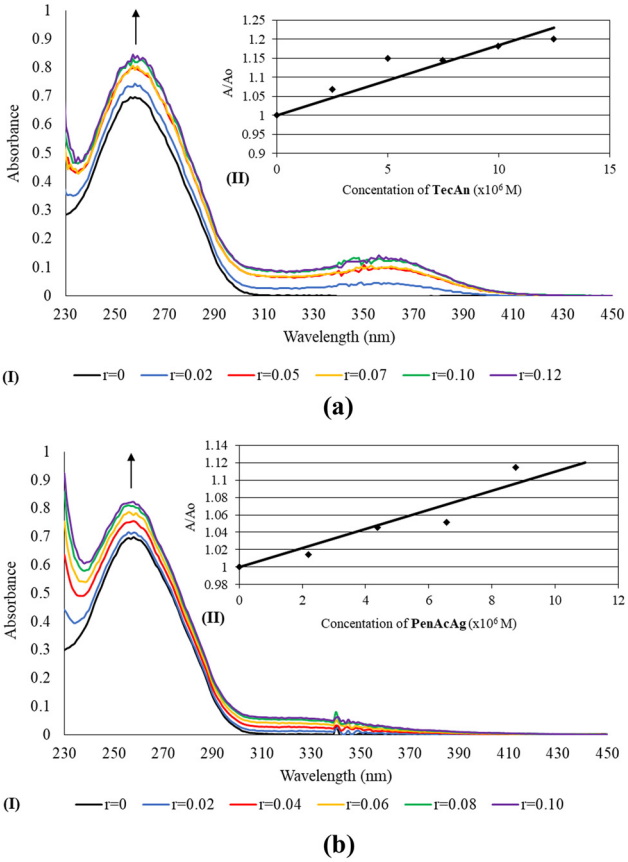

Figure 8: (I) UV-Vis spectra of CT-DNA in buffer solution in the absence and presence of **TecAn** (a) and **PenAcAg** (b) at various *r* values (0, 0.02, 0.05, 0.07, 0.10, and 0.12; *r* = [complex]/[DNA], [DNA] = 10^{-4} M) and (II) plot of A/Ao vs [complex] at 258 nm.

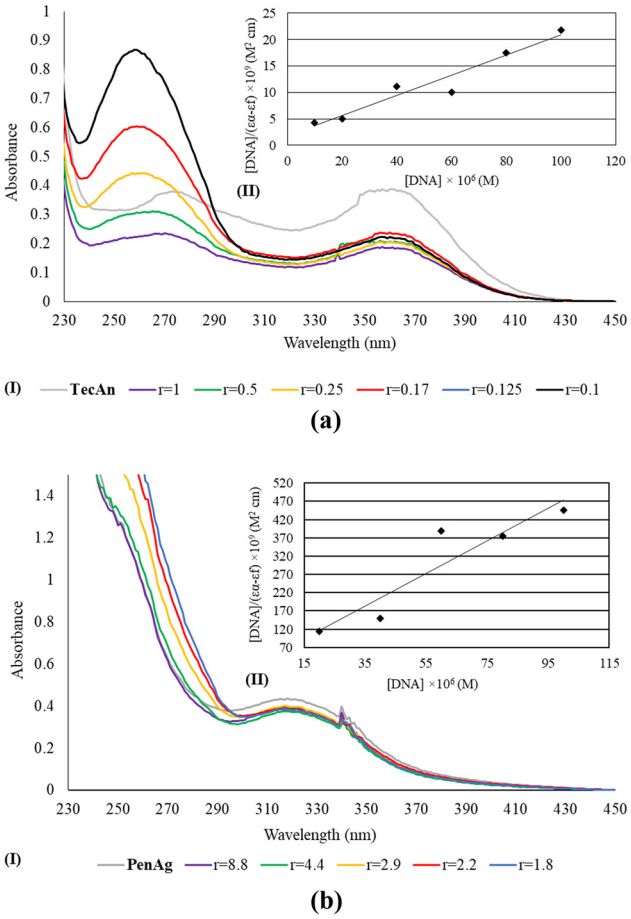

Figure 9: (I) UV spectra of **TecAn** (a) and **PenAcAg** (b) in the absence and presence of CT DNA at *r* values 1, 0.5, 0.25, 0.17, 0.125, and 0.1 for **TecAn** and 8.8, 4.4, 2.9, 2.2, and 1.8 for **PenAcAg** (r = [complex]/[DNA], [complex] = 25 μM (**TecAn**) and 218 μM (**PenAcAg**), [CT DNA] = 10–100 μM). (II) Graphical plot of [DNA]/(ε_α–ε_f) vs [DNA].

at 370–380 nm, with increasing concentration of CT-DNA (Figure 9). K_b is obtained from the ratio of the slope to the y intercept in plots [DNA]/(ε_A-ε_f) vs [DNA], according to the following equation (Banti et al., 2015, 2016; Chrysouli et al., 2018; Polychronis et al., 2019; Stathopoulou et al., 2021):

$$\frac{[DNA]}{(\varepsilon_A - \varepsilon_f)} = \frac{[DNA]}{(\varepsilon_b - \varepsilon_f)} + \frac{1}{K_b(\varepsilon_b - \varepsilon_f)} \quad (1)$$

where [DNA] is the concentration of CT-DNA, $\varepsilon_A = A_{obsd}$/[compound], ε_f is the extinction coefficient for the free compound, and ε_b is the extinction coefficient for the compound in the fully bound form (Banti et al., 2015, 2016; Chrysouli et al., 2018; Polychronis et al., 2019; Stathopoulou et al., 2021). The DNA binding constant (K_b) for **TecAn** is (11.1 ± 0.5) × 10^4 M^{-1} and for **PenAcAg** is (15.6 ± 5.1) × 10^4 M^{-1}. Moreover, the K_b value of tetracycline ($TecH_2$) is (7.2 ± 0.8) × 10^4 M^{-1}. Therefore, the conjugation of $TecH_2$ and PenH to antimony(V) and silver(I), respectively, form new agents that significantly bind DNA.

2.11.1.2 Fluorescence spectroscopic studies

The binding properties of **TecAn** and **PenAcAg** towards DNA were studied further by fluorescent spectroscopy. EB is a strong intercalator of DNA and for this reason it emits intense fluorescent light in the presence of DNA. The quenching of the emitted light when EB is displaced from the CT-DNA-EB complex by an agent indicates an intercalative or minor groove type of binding between DNA and the compound. The CT-DNA-EB complex emits at λ_{max} = 588 nm upon its excitation at λ_{ex} = 527 nm (Banti et al., 2016, 2021; Kapetana and Banti, 2022; Latsis et al., 2018; Stathopoulou et al., 2021). The fluorescence spectra of the CT-DNA-EB compound with the increasing concentrations of **TecAn** or **PenAcAg** (0–600 μM) are shown in Figure 10. The fluorescence emitted from the CT-DNA-EB complex at 588 nm undergoes a 20.3% (**TecAn**) and 37.4% (**PenAcAg**) quenching upon increasing the concentrations with respect to the initial fluorescence

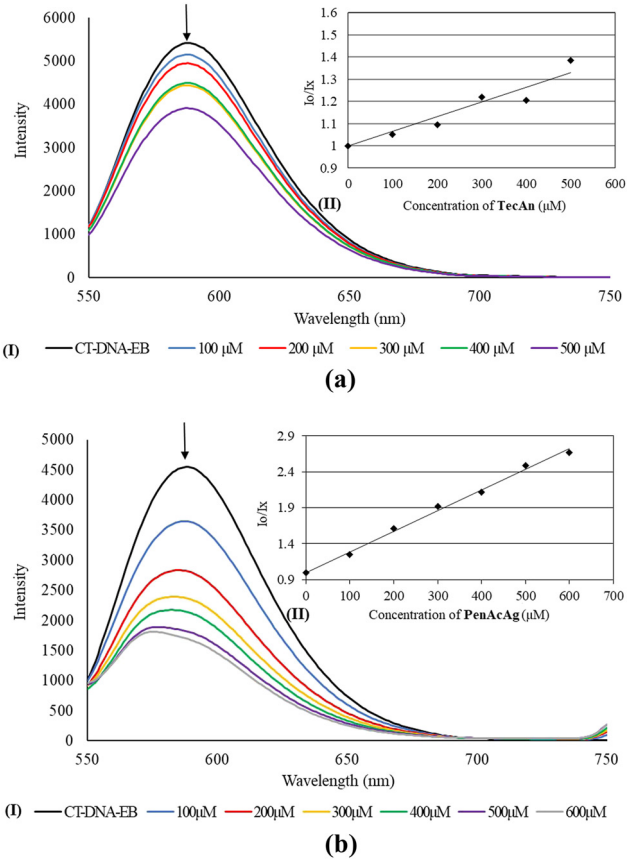

Figure 10: (I) Emission spectrum of CT-DNA-EB complex in the presence of **TecAn** (a) and **PenAcAg** (b) ([EB] = 2.3 μM [DNA] = 26 μM [complex] = 0–600 μM) λ_{ex} = 527 nm. The arrow shows that the intensity changes upon increasing the complex concentration. (II) Inset shows the plots of emission intensity I_o/I_x vs [complex].

intensity of the solutions without the agent. The binding constant (K_{app}) was calculated using the equation (Banti et al., 2016, 2021; Kapetana and Banti, 2022; Latsis et al., 2018; Stathopoulou et al., 2021):

$$K_{EB}[EB] = K_{app}[drug] \quad (2)$$

where [drug] is the concentration of the agent at a 50% reduction of the fluorescence, $K_{EB} = 10^7\ M^{-1}$, and the concentration of [EB] is 2.3 μM. The concentration of the drug at a 50% reduction of the fluorescence is derived from the diagram of I_0/I_x *vs* the concentration of **TecAn** or **PenAcAg** (Figure 10), where I_0 and I_x are the fluorescence intensities of the CT-DNA in the absence and presence of the compound. K_{SV} is the Stern–Volmer quenching constant and [Q] is the concentration of the quencher (Banti et al., 2016, 2021; Kapetana and Banti, 2022; Latsis et al., 2018; Stathopoulou et al., 2021). The linear Stern–Volmer equation is the following:

$$I_0/I = 1 + K_{SV} \times [Q] \quad (3)$$

The apparent binding constant K_{app} calculated for **TecAn** is $(1.1 \pm 0.2) \times 10^4\ M^{-1}$, while the corresponding value for **PenAcAg** is $(6.7 \pm 1.1) \times 10^4\ M^{-1}$. In addition, the K_{app} constant of tetracycline ($TecH_2$) is $(0.8 \pm 0.4) \times 10^4\ M^{-1}$, TPSb is $(5.3 \pm 0.5) \times 10^4\ M^{-1}$, and PenNa is $(0.9 \pm 0.1) \times 10^4\ M^{-1}$. These values are lower than the binding constants of the classical intercalators EB ($10^6\ M^{-1}$), confirming the groove binding of both metallodrugs.

2.11.1.3 Viscosity measurement

The interaction of DNA with an anticancer agent affects the length of DNA which consequently changes the viscosity of its solution (Banti et al., 2021; Kapetana and Banti, 2022; Latsis et al., 2018). Thus, (i) if the agent intercalates with the DNA strands, lengthening of the DNA occurs with an increase in the solution viscosity, (ii) if the agent interacts electrostatically with the DNA, this results in no effect on the DNA length and no significant change in viscosity; (iii) in the case of cleavage of the DNA strands, the length of the DNA decreases along with the viscosity, and (iv) if the agent binds the DNA helix binding covalently with it, decrease in the viscosity is exhibited (Banti et al., 2021; Kapetana and Banti, 2022; Latsis et al., 2018). The relative DNA length (L/L_0) is calculated from the equation:

$$L/L_0 = (n/n_o)^{1/3} \quad (4)$$

where $(n/n_0)^{1/3}$ shows the relative specific viscosity of the DNA solutions. Solution of CT-DNA (10 mM) is incubated with the increasing amounts of **TecAn** and **PenAcAg**. Figure 11 shows the relative specific viscosity $(n/n_0)^{1/3}$ vs binding ratio. The negligible decrease in the viscosity of DNA solution, upon increasing the concentrations in the case of **TecAn**, and the less pronounced increase in the case of **PenAcAg**, suggests a groove binding mode of both metallodrugs (Banti et al., 2021; Kapetana and Banti, 2022; Latsis et al., 2018). This is in agreement with the findings extracted from UV-Vis and fluorescence studies.

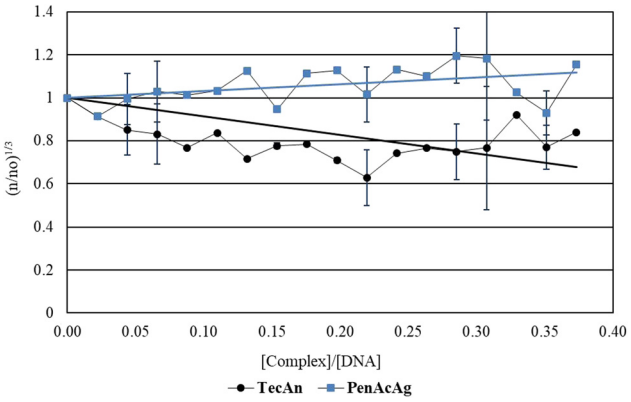

Figure 11: Effect of increasing concentrations of **TecAn** and **PenAcAg** on the relative viscosity of CT-DNA at 25°C. ([DNA] = 10 mM, r = [compound]/[DNA], n is the viscosity of DNA in the presence of **TecAn** and **PenAcAg** and n_o is the viscosity of DNA alone).

2.12 Study of the peroxidation of linoleic acid by the enzyme LOX

LOX is an enzyme that is mainly distributed in the mitochondrion, and it causes apoptosis. LOX oxidizes linoleic acid to hyperoxo-linoleic acid during the inflammation mechanism. In order to clarify whether the apoptosis caused to the MCF-7 (HD) cells is due to the direct interaction between the agents with DNA or to the mitochondrion dysfunction, which consequently activates the intrinsic pathway of apoptosis through caspases, the LOX inhibitory activity of **TecAn** or **PenAcAg** is studied (Banti et al., 2016, 2021; Chrysouli et al., 2018). The hyperoxo-linoleic acid formed is monitored by recording the increase in the absorbance at 234 nm. The degree of LOX activity (A, %) by the influence of **TecAn** or **PenAcAg** was calculated by equation:

$$A\ (\%) = 100 \times (u_o \text{ in the presence of inhibitor}) / (u_o \text{ in the absence of inhibitor}) \quad (5)$$

The value of the initial velocity (u_o, $mM \cdot s^{-1}$) was computed by the formula:

$$\upsilon_o = \Delta C/\Delta t = \Delta A/(\Delta t \times \varepsilon) = \text{tga}/(\Delta t \times \varepsilon) \quad (6)$$

where C is the concentration of the oxidation product of linoleic acid (hydroperoxy–linoleic acid), t is the reaction time, ε is the molar absorbance coefficient of hydroperoxy–linoleic acid, and tga is the slope of the kinetic curve displayed as absorbance vs time.

Figure 12 shows LOX activity (A%) vs various concentrations of **TecAn** and **PenAcAg**. The IC_{50} value for **PenAcAg** is 19.8 μM whereas no IC_{50} value was determined for **TecAn** at the concentrations tested (up to 60 μM) (Figure 12). For comparison, the corresponding IC_{50} values of cisplatin is 65.9 μM, while the corresponding values for PenNa and $TecH_2$ are higher than 40 μM (Banti et al., 2016, 2021; Chrysouli et al., 2018; Poyraz et al., 2011). Therefore, a different mechanism of action between **TecAn** or **PenAcAg** may be expected.

The reversible or irreversible type of inhibition was investigated by incubating the substrate with the inhibitor before adding the enzyme at various times (Banti et al., 2012). The effect on the enzyme activity of different incubation duration of the substrate with a constant complex concentration supports an irreversible kind of inhibition (Figure S14).

The kind of inhibitor type was evaluated by the steady-state kinetics at different substrate concentrations (ranging from 0.01 to 0.1 mM) in the absence and presence of **PenAcAg** (19.8 mM). A graphical method with Lineweaver–Burk coordinates (double reciprocal method) was used (Figure 13). From the slope and intercept of the linear graph, the kinetic parameters (K_m and V_{max}) were determined. The K_m and V_{max} values of free enzyme are 0.035 mM and 27.5 mM·s^{-1}, respectively. The apparent values in the presence of **PenAcAg** are K_m = 0.14 mM and V_{max} = 20.7 mM·s^{-1} suggesting that **PenAcAg** inhibits the enzyme via a mixed inhibition mechanism (higher K_m value and lower V_{max}) (Xanthopoulou et al., 2008). In this mechanism, both the EI (enzyme-inhibitor) and ESI (enzyme-substrate-inhibitor) complexes are formed (Xanthopoulou et al., 2008). This occurs when the inhibitor binds to a place other than the substrate binding site, resulting in a decrease in catalytic rate and perhaps cell death. These inhibitors could not be used as anti-inflammatory drugs (Xanthopoulou et al., 2008).

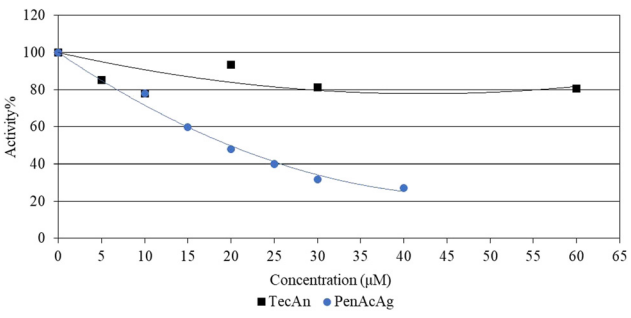

Figure 12: LOX activity (A%) *vs* various concentrations of **TecAn** and **PenAcAg**.

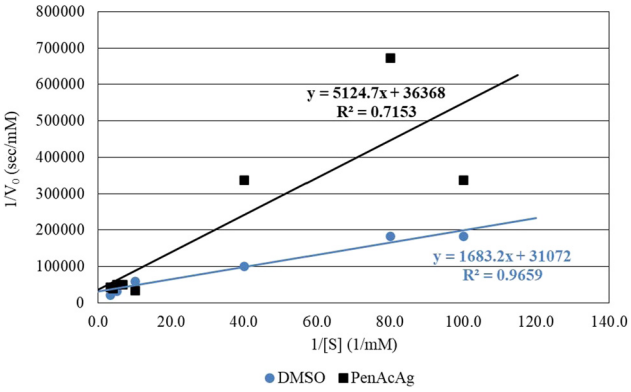

Figure 13: Graphical plotting for determination of K_m and V_{max} using Lineweaver–Burk coordinates for **PenAcAg**.

2.13 Reaction of TecAn with GSH

Antileishmanial drugs include pentavalent antimonials (Sharma et al, 2008). In this case antimony(v) is a prodrug which is reduced to active antimony(iii) by the tripeptide GSH (Ozturk et al., 2007; Sharma et al, 2008). Sb(v) is biologically less active, while Sb(iii) is the active form of antimonials (Ozturk et al., 2007, 2009, 2010). GSH on the other hand is over-expressed in tumor cells (e.g., its concentration is twice in breast cancer cells than that found in normal ones). It plays a vital role in protecting cancer cells and it is the reason for the resistance they develop against chemotherapy (Banti et al. 2014; Syng-Ai et al., 2004). Therefore, the use of low toxic Sb(v) species which are converted to the active Sb(iii) ones in cancer cells by the GSH is expected to lead to new chemotherapeutics with high selectivity against cancer cells than normal ones. Therefore, the redox reaction between the GSH and **TecAn** is studied, here, using vibrational spectroscopy The vibrational band of the S–H bond in the ATR-FTIR spectrum of GSH (Figure S15) is absent when it is oxidized by H_2O_2 (1:1 molar ratio) due to the formation of the disulfide GS-SG. (Figure S15) (Shayani-Jama and Nematollahi, 2010). When H_2O_2 is replaced by **TecAn** under the same reaction conditions, the formation of the disulfide with the elimination of the ν(S–H) vibrational band occurs as well (Figure S5) (Kapetana and Banti, 2022).

3 Conclusion

Antibiotics induce cancer cell apoptosis through breakage of DNA strands since DNA is one of their major molecular targets. Thus, the conjugates of tetracycline with antimony(v) **TecAn** and the corresponding one of penicillin with silver **PenAcAg** were prepared and tested *in vitro* against human breast adenocarcinoma cell lines: MCF-7 (positive to hormones receptor (HR+)), MDA-MB-231 (negative to hormones receptor (HR−)). **TecAn** and **PenAcAg** inhibit both cell lines in a similar manner implying that hormone receptors play no role in their mechanism of action. Although, **TecAn** and **PenAcAg** are classified as toxic agents, according to FDA criteria, they are both significantly more effective against cancerous cells than normal cells compared to cisplatin which, however, is an anticancer drug in clinical use. **TecAn** and **PenAcAg** induce apoptosis at 56.2 ± 0.2% (**TecAn**) and 49.3 ± 0.6% (**PenAcAg**) of MCF-7 (HD) cells, respectively, like cisplatin, where the percentage of apoptotic cells rises up to 96.5%. Electronic absorption and fluorescent spectroscopic data suggest that both conjugates interact strongly with DNA through groove binding mode. The results are confirmed by the meaningless perturbation in the viscosity of DNA solution when it is treated with **TecAn** and **PenAcAg**. GSH readily reduces antimony(v) to highly toxic antimony(iii). **TecAn** reacts with GSH in a redox reaction where the biological inactive Sb(v) turns in the active Sb(iii). GSH is a cysteine containing tripeptide, over-expressed in the cancer cells. It removes metal-chemotherapeutics from the cytoplasm, preventing their efficient interaction with crucial intracellular components (DNA, mitochondrion, etc.) and developing resistance in cancer cells toward chemotherapy. However, this is cancelled by the active Sb(iii) species formed from the reaction of TecAn with GSH in the cancer cells cytoplasm converting their defending tool to a disadvantage. **PenAcAg**, on the other hand, inhibits LOX activity stronger than cisplatin suggesting the activation of the apoptosis pathway through mitochondrion.

Experimental

Materials and instruments

All solvents used were of reagent grade and were used with no further purification. Triphenyl antimony, silver nitrate, tetracycline, sodium penicillin, LOX, and linoleic acid were purchased from Aldrich-Merck and they were used without any further purification. DMSO was purchased from Riedel-de Haën. Dulbecco's modified Eagle's medium, (DMEM), fetal bovine serum, glutamine, and trypsin were purchased from Gibco, Glasgow, UK. Phosphate buffer saline (PBS), CT-DNA, EB, and propidium iodide were purchased from Sigma-Aldrich. Melting point was measured in open tubes with a STUART SMP30 scientific apparatus, and it is uncorrected. Mid-infrared spectra (4,000–400 cm^{-1}) were obtained on Cary 670 FTIR spectrometer (Agilent Technologies). The fluorescence spectra were recorded on a Jasco FP-8200 Fluorescence Spectrometer. TG–DTA was carried out on a DTG/TG NETZSCH STA 449 C apparatus, under air flow (with a heating rate of 10°C·min^{-1} (25–500°C). ^{1}H and ^{13}C NMR spectra were recorded with a Bruker AC 400 MHz FT-NMR instrument in DMSO-d_6 solution. A UV-1600 PC series spectrophotometer of VWR was used to obtain electronic absorption spectra. XRF measurement was carried out with Rigaku NEX QC EDXRF analyzer (Austin, TX, USA).

Synthesis of TecAn

0.176 g Ph_3Sb(iii) (0.5 mmol) were oxidized by 0.05 mL of H_2O_2 30% hydrogen peroxide in the presence of 0.222 g tetracycline (0.5 mmol) in 20 mL of Et_2O. The solution was stirred in ice bath at 4°C for 5 h. The pale-yellow precipitation was filtered off and dried at ambient conditions. The powder product was dissolved in 20 mL of MeCN followed by filtration to remove the impurities. The clear solution was concentrated to dryness in the rotary evaporator and the solid powder **TecAn** was washed with 2 mL of Et_2O.

TecAn: pale-yellow powder; yield 51%; melting point: 149–154°C; MW = 795.435 g·mol^{-1}. Elemental analysis found: C: 60.10; H: 4.85; N: 3.72; Sb: 14.86 (±0.09)% w/w. Calculated for $C_{40}H_{38}N_2O_8Sb$, C = 60.32; H = 4.80; N = 3.52, Sb = 15.29% w/w; ATR-IR (cm^{-1}): 3,052 w, 1,618 m, 1,480 w, 1,432 m, 1,379 w, 1,215 w, 1,175 m, 1,092 m, 1,066 m, 995 m, 857 m, 738 s, 693 s, 618 w, 570 w, 511 w, 451 s, and 414 s. ^{1}H NMR (ppm) in DMSO-d_6: 9.21 OC(1) NH_2, 7.54 C(8)-H, 7.13 C(9)-H, 6.92 C(7)-H, 4.87 C(10)-OH, 2.85 C(10a)-H, 2.5 C(15)-C(16)-H, 1.96 C(11)-H, and 1.51 C(14)-H; ^{13}C NMR (ppm) in DMSO-d_6: 190.2 (C5), (C3), (C15), 172.5 (C4), 168.9 (C1), 162.9 (C6), 147.7 (C9a), 143.8 (C8), 117.3 (C9), 116.8 (C7), 114.3 (C5a), 103.7 (C4a), 73.3 (C3a), 68.5 (C10), 43.1 (C15), (C16), 34.6 (C10a), 26.4 (C11a), and 23.5 (C11); UV-Vis (DMSO): λ_{max} (logε) = 378 nm (4.21), 304 nm (4.14), and 266 nm (4.11).

Synthesis of PenAcAg

A ddw solution of silver nitrate (0.5 mmol, 0.085 g) was added to a methanolic solution of benzyl-penicillin sodium (PenNa) (0.5 mmol, 0.178 g) and the resulting suspension was stirred for 5 min. The yellowish precipitation was filtered off. The powder product was dissolved in 20 mL of MeCN and the insoluble impurities were removed with centrifugation at 2,000 rpm. The clear supernatant was concentrated to give the **PenAcAg**.

PenAcAg: yellow powder; yield 20%; melting point: 121–125°C, MW = 964 g·mol^{-1}. Elemental analysis found: C = 44.55; H = 4.43; N = 8.95; S = 6.74; Ag = 19.81 (±0.27)% w/w. Calculated for $C_{36}H_{40}Ag_2O_8N_6S_2$, C = 44.83; H = 4.18; N = 8.71; S = 6.67; Ag = 22.37% w/w; ATR-IR (cm^{-1}): 3,267 m, 2,960 s, 2,927 s, 2,859 s, 1,767 s, 1,659 w, 1,576 m, 1,454 m, 1,394 m, 1,311 m, 1,249 m, 1,088 s, 1,029 m, 890 s, 756 s–m, 697 s, 566 s, and 458 s. ^{1}H NMR (ppm) in DMSO-d_6: 8.81 [NH–C(6)═O]–H, 7.32–7.22 (Benzyl)-H, 5.48 C(9)-H, 5.40 C(8)-H, 4.14 C(12)-H, 3.55 C(5)-H, 2.09 (MeCN)-H, 1.60 C(16)-H, and 1.48 C(17)-H. UV-Vis (DMSO): λ_{max} (log ε) = 269 nm (3.78).

Biological tests

The biological tests were performed as described previously (Banti et al., 2015, 2016, 2021; Chrysouli et al., 2018; Kapetana and Banti, 2022; Latsis et al., 2018; Polychronis et al., 2019; Stathopoulou et al., 2021; Tsiatouras et al., 2016).

SRB assay

This study was performed according to the procedure reported previously (Banti et al., 2015, 2016, 2021; Chrysouli et al., 2018; Kapetana and Banti, 2022; Latsis et al., 2018; Polychronis et al., 2019; Stathopoulou et al., 2021; Tsiatouras et al., 2016).

Evaluation of *in vitro* genotoxicity with MN assay

The evaluation of genotoxicity caused by **TecAn** and **PenAcAg** was performed following the protocol reported elsewhere (Banti et al., 2015, 2016; Kapetana and Banti, 2022; Polychronis et al., 2019; Stathopoulou et al., 2021).

Evaluation of *in vivo* toxicity with brine shrimp (*Artemia salina*) assay

Brine shrimp assay was performed as previously reported (Banti and Hadjikakou, 2021).

Cell morphology studies

MCF-7 cells' morphology was observed under an inverse microscope, as previously reported (Banti et al., 2015, 2016; Kapetana and Banti, 2022; Polychronis et al., 2019; Stathopoulou et al., 2021).

AO/EB staining was used to detect apoptosis: Banti et al. (2015), Kapetana and Banti (2022), and Stathopoulou et al. (2021).

DNA binding studies

UV-Vis studies: this study was performed as described previously (Banti et al., 2015, 2016; Chrysouli et al., 2018; Polychronis et al., 2019; Stathopoulou et al., 2021).

Fluorescence studies: this study was performed as described previously (Banti et al., 2016, 2021; Kapetana and Banti, 2022; Latsis et al., 2018; Stathopoulou et al., 2021).

Viscosity measurements: this study was carried out as previously reported (Banti et al., 2021; Kapetana and Banti, 2022; Latsis et al., 2018).

LOX activity inhibition

This study was performed as previously reported (Xanthopoulou et al., 2006).

Acknowledgments: (a) This work was carried out in partial fulfilment of the requirements for the Master thesis of Ms Z-CMF according to the curriculum of the International Graduate Program in "Biological Inorganic Chemistry," which operates at the University of Ioannina within the collaboration of the Departments of Chemistry of the Universities of Ioannina, Athens, Thessaloniki, Patras, Crete and the Department of Chemistry of the University of Cyprus (http://bic.chem.uoi.gr/BIC-En/index-en.html) under the supervision of Prof. Sotiris K. Hadjikakou. (b) This work was carried out in partial fulfilment of the requirements for the Master thesis of Ms PZT under the supervision of Prof. Sotiris K. Hadjikakou. (c) PZT acknowledges the financial support from the Eugenides Foundation for a scholarship for her postgraduate studies.

Funding information: Authors state no funding involved.

Author contributions: Paraskevi Z. Trialoni: investigation; Zografia-Christina M. Fyrigou: investigation; Christina N. Banti: investigation, methodology, writing – original draft,

and writing – review and editing; Sotiris K. Hadjikakou: conceptualization, methodology, supervision, validation, writing – original draft, and writing – review and editing.

Conflict of interest: Authors state no conflict of interest.

Data availability statement: All data generated or analyzed during this study are included in this published article and its supplementary information files.

References

Abughazaleh R.D., Tracy T.S., 2014, In: Balakrishnan N., Colton T., Everitt B., Piegorsch W., Ruggeri F, Teugels JL (eds), Therapeutic Index. Wiley StatsRef: Stat. Ref. Online. doi: 10.1002/97811 18445 112.stat07121.

Afsar T., Trembley J., Salomon C., Razak S., Khan M.R., Ahmed K., Growth inhibition and apoptosis in cancer cells induced by polyphenolic compounds of Acacia hydaspica: involvement of multiple signal transduction pathways. Sci. Rep., 2016, 6, 23077.

Anacona J.R., Figueroa E.M., Synthesis and characterization of metal complexes with penicillin. J. Coord. Chem., 1999, 48, 181.

Banti C.N., Giannoulis A.D., Kourkoumelis N., Owczarzak A.M., Poyraz M., Kubicki M., et al., Mixed ligand–silver (I) complexes with anti-inflammatory agents which can bind to lipoxygenase and calf-thymus DNA, modulating their function and inducing apoptosis. Metallomics, 2012, 6, 545–60.

Banti C.N., Kyros L., Geromichalos G.D., Kourkoumelis N., Kubicki M., Hadjikakou S.K., A novel silver iodide metalo-drug: Experimental and computational modelling assessment of its interaction with intracellular DNA, lipoxygenase and glutathione. Eur. J. Med. Chem., 2014, 77, 388.

Banti C.N., Charalampou D.C., Kourkoumelis N., Owczarzak A.M., Kubicki M., Hadjikakou S.K., et al., Mono-nuclear cis-Pd(II) chloride complex of the thio-nucleotide analogue 5-methylthiouracil and its biological activity. Polyhedron, 2015, 87, 251–258.

Banti C.N., Papatriantafyllopoulou C., Manoli M., Tasiopoulos A.J., Hadjikakou S.K., Nimesulide silver metallodrugs, containing the mitochondriotropic, triaryl derivatives of pnictogen; anticancer activity against human breast cancer cells. Inorg. Chem., 2016, 6, 8681.

Banti C.N., Hadjikakou S.K., Evaluation of toxicity with brine shrimp assay. Bio-protocol, 2021, 11, e3895.

Banti C.N., Raptopoulou C.P., Psycharis V., Hadjikakou S.K., Novel silver glycinate conjugate with 3D polymeric intermolecular self-assembly architecture; an antiproliferative agent which induces apoptosis on human breast cancer cells. J. Inorg. Biochem., 2021, 216, 111351.

Ben Salem I., Mezni M., Boulila A., Hamdi M., Saidi M., Removal of penicillin G and erythromycin with ionizing radiation followed by biological treatment. Curr. Microbiol., 2016, 73, 582.

Bhattacharya B., Mukherjee S., Cancer therapy using antibiotics. J. Cancer Ther., 2015, 6, 849.

Bordner J., Doak G.O., Everett T.S., Crystal structure of 2,2,4,4-Tetrahydro-2,2,2,4,4,4-hexaphenyl-1,3,2,4-dioxadistibetane (Triphenylstibine Oxide Dimer) and related compounds. J. Am. Chem. Soc., 1986, 108, 4206.

Branch S.K., Casy A.F., Ominde E.M., Application of 1H nuclear magnetic resonance spectroscopy to the analysis of β-lactam antibiotics and their common degradation products. J. Pharm. Biomed. Anal., 1987, 5, 73.

Christowitz C., Davis T., Isaacs A., van Niekerk G., Hattingh S., Engelbrecht A.-M., Mechanisms of doxorubicin-induced drug resistance and drug resistant tumour growth in a murine breast tumour model. BMC Cancer, 2019, 19, 1–10.

Chrysouli M.P., Banti C.N., Kourkoumelis N., Panayiotou N., Tasiopoulos A.J., Hadjikakou S.K., Chloro(triphenylphosphine) gold(I) a forefront reagent in gold chemistry as apoptotic agent for cancer cells. J. Inorg. Biochem., 2018, 179, 107–120.

Fuoco D., Classification framework and chemical biology of tetracycline-structure-based drugs. Antibiotics, 2012, 1, 1–13.

Gao Y., Shang Q., Li W., Guo W., Stojadinovic A., Mannion C., et al. Antibiotics for cancer treatment: A double-edged sword. J. Cancer, 2020, 11, 5135.

Gottlieb H.E., Kotlyar V., Nudelman A., NMR chemical shifts of common laboratory solvents as trace impurities. J. Org. Chem., 1997, 62, 7512–7515.

Jaksic Z., Biochemical and biological effects of organotins, Chapter 10, mechanisms organotin-induced apoptosis, Bentham Science Publishers, Netherlands, 2012, pp. 149–163.

Kapetana M., Banti C.N., Papachristodoulou C., Psycharis V., Raptopoulou C., Hadjikakou S.K., Conjugation of triphenylantimony(V) with carvacrol against human breast cancer cells. J. Biol. Inorg., 2022, 27, 373–389.

Ketikidis I., Banti C.N., Kourkoumelis N., Tsiafoulis C.G., Papachristodoulou C., Kalampounias A.G., et al., Conjugation of penicillin-G with silver(I) ions expands its antimicrobial activity against gram negative bacteria. Antibiotics, 2020, 9, 25.

Latsis G.K., Banti C.N., Kourkoumelis N., Papatriantafyllopoulou C., Panagiotou N., Tasiopoulos A., et al., Poly organotin acetates against DNA with possible implementation on human breast cancer. Int. J. Mol. Sci., 2018, 19, 2055–2072.

Leypold C.F., Reiher M., Brehm G., Schmitt M.O., Schneider S., Matousek P., et al., Tetracycline and derivatives – assignment of IR and Raman spectra via DFT calculations. Phys. Chem., 2003, 5, 1149–1157.

Llewellyna A., Howarda C., McCabea C., An exploration of the experiences of women treated with radiotherapy for breast cancer: Learning from recent and historical cohorts to identify enduring needs. Eur. J. Oncol. Nurs., 2019, 39, 47–54.

Macy E., Penicillin and beta-lactam allergy: epidemiology and diagnosis. Curr. Allergy Asthma Rep., 2014, 14, 476.

Mealey K.L., Barhoumi R., Burghardt R.C., Safe S., Kochevar D.T., Doxycycline induces expression of P glycoprotein in MCF-7 breast carcinoma cells. Antimicrob. Agents Chemother., 2002, 46, 755–761.

Naqvi S., Mohiyuddin S., Gopinath P., Niclosamide loaded biodegradable chitosan nanocargoes: an *in vitro* study for potential application in cancer therapy. R. Soc. Open. Sci., 2017, 4, 170611.

Ozturk I.I., Hadjikakou S.K., Hadjiliadis N., Kourkoumelis N., Kubicki M., Baril M., et al., Synthesis, structural

characterization and biological studies of new antimony(III) complexes with thioamides. The influence of the solvent on the geometry of the complexes. Inorg. Chem., 2007, 46, 8652–8661.

Ozturk I.I., Hadjikakou S.K., Hadjiliadis N., Kourkoumelis N., Kubicki M., Tasiopoulos A.J., et al., New Antimony(III) bromide complexes with thioamides: synthesis, characterization, and cytostatic properties. Inorg. Chem., 2009, 48, 2233.

Ozturk I., Filimonova S., Hadjikakou S.K., Kourkoumelis N., Dokorou V., Manos E., et al., Structural motifs and biological studies of new antimony(III) iodide complexes with thiones. Inorg. Chem., 2010, 49, 488.

Ozturk I.I., Banti C.N., Kourkoumelis N., Manos M.J., Tasiopoulos A.J., Owczarzak A.M., et al., Synthesis, characterization and biological activity of antimony(III) or bismuth(III) chloride complexes with dithiocarbamate ligands derived from thiuram degradation. Polyhedron, 2014, 67, 89–103.

Polychronis N.M., Banti C.N., Raptopoulou C.P., Psycharis V., Kourkoumelis N., Hadjikakou S.K., Non steroidal anti-inflammatory drug (NSAIDs) in breast cancer chemotherapy; antimony(V) salicylate a DNA binder. Inorg. Chim. Acta, 2019, 489, 39–47.

Poyraz M., Banti C.N., Kourkoumelis N., Dokorou V., Manos M.J., SimčičM., et al., Synthesis, structural characterization and biological studies of novel mixed ligand Ag(I) complexes with triphenylphosphine and aspirin or salicylic acid. Inorg. Chim. Acta., 2011, 375, 114–121.

Psomas G., Mononuclear metal complexes with ciprofloxacin: Synthesis, characterization and DNA-binding properties. J. Inorg. Biochem., 2008, 1798–1811.

Rocha C.R., Silva M.M., Quinet A., Cabral-Neto J.B., Menck C.F., DNA repair pathways and cisplatin resistance: an intimate relationship. Clinics, 2018, 6, 73.

Sharma P., Perez D., Cabrera A., Rosas N., Arias J.L., Perspectives of antimony compounds in oncology. Acta Pharmacol. Sinm, 2008, 29, 881.

Shayani-Jama H., Nematollahi D., Electrochemical evidences in oxidation of acetaminophen in the presence of glutathione and N-acetylcysteine. Chem. Commun., 2010, 46, 409.

Stathopoulou M.E.K., Zoupanou N., Banti C.N., Douvalis A.P., Papachristodoulou C., Marousis K.D., et al., Organotin derivatives of cholic acid induce apoptosis into breast cancer cells and interfere with mitochondrion; Synthesis, characterization and biological evaluation. Steroids, 2021, 167, 108798.

Syng-Ai C., Leela Kumari A., Khar A., Effect of curcumin on normal and tumor cells: Role of glutathione and Bcl-2. Mol. Cancer Ther., 2004, 3, 1101.

The Cancer Genome Atlas Network. Comprehensive molecular portraits of human breast tumours. Nature, 2012, 490, 61–70.

Tsiatouras V., Banti C.N., Grześkiewicz A.M., Rossos G., Kourkoumelis N., Kubicki M., et al., Structural, photolysis and biological studies of novel mixed metal Cu(I)-Sb(III) mixed ligand complexes. J. Photochem. Photobiol. B, 2016, 163, 261–268.

Williamson D.E., Everett, Jr. G.W., A proton nuclear magnetic resonance study of the site of metal binding in tetracycline. J. Am. Chem. Soc., 1975, 97, 2397.

Xanthopoulou M.N., Hadjikakou S.K., Hadjiliadis N., Kubicki M., Karkabounas S., K.Charalabopoulos, et al., Synthesis and characterization of a new chloro-di-phenyltin(IV) complex with thioamide 2-mercapto-nicotinic acid. Study of its influence upon the catalytic oxidation of linoleic acid to hydroperoxylinoleic acid by the enzyme Lipoxygenase. J. Organomet. Chem., 2006, 691, 1780.

Xanthopoulou M.N., Hadjikakou S.K., Hadjiliadis N., Milaeva E.R., Gracheva J.A., Tyurin V.Y., et al., Biological studies of new organotin (IV) complexes of thioamide ligands. Eur. J. Med. Chem., 2008, 43, 327.